Original Article

Gamma ray exposure buildup factor and shielding features for some binary alloys using MCNP-5 simulation code

Y.S. Rammah [a], K.A. Mahmoud [b, c], Faras Q. Mohammed [d], M.I. Sayyed [e, f, *], O.L. Tashlykov [b], R. El-Mallawany [a]

[a] Physics Department, Faculty of Science, Menoufia University, Shebin El-Koom, 32511, Menoufia, Egypt
[b] Ural Federal University, St. Mira, 19, 620002, Yekaterinburg, Russia
[c] Nuclear Materials Authority, Maadi, Cairo, Egypt
[d] Nanotechnology and Advanced Materials Research Center, University of Technology, 35010, Baghdad, Iraq
[e] Department of Physics, Faculty of Science, Isra University, Amman, Jordan
[f] Department of Nuclear Medicine Research, Institute for Research and Medical Consultations (IRMC), Imam Abdulrahman Bin Faisal University (IAU), PO Box 1982, Dammam, 31441, Saudi Arabia

ARTICLE INFO

ABSTRACT

Gamma radiation shielding features for three series of binary alloys identified as (Pb–Sn), (Pb–Zn), and (Zn–Sn) have been investigated. The mass attenuation coefficients (μ/ρ) for the selected alloys were simulated using the MCNP-5 code in the energy range between 0.01 and 15 MeV. Moreover, the (μ/ρ) values were computed using WinXCOM database in the same energy range to validate the simulation results. Results reveal a good agreement between the simulated and computed values. The half value layer (HVL), mean free path (MFP), effective atomic number (Z_{eff}) and exposure buildup factor (EBF) were evaluated for the selected binary alloys. Results showed that the PS1, PZ1, and ZS2 alloys have the best shielding parameters and better than the commercially standard and available radiation shielding materials. Therefore, the investigated alloys can be used as effective radiation shielding materials against gamma ray with energies between 0.01 and 15 MeV.

1. Introduction

Currently, radioactive isotopes have more attractive applications in several technological fields such as; radiotherapy, radiology, nuclear medicines, industry to test the void and insertion into the inner part of the material, and agricultural to distinguish between various wood types. On the other hand, radiations like γ-rays and neutrons have dangerous effects on the environment, animals, and humans. For the reasons mentioned above, several researchers are interested in finding out better materials to be used as a promise radiation shielding materials [1–8]. It is well known that in order to reduce the exposure of the harmful radiation, the shielding material is planted between the radioactive source and the workers or the environment. The materials to be used as effective radiation shielding must be possessed space homogeneity of composition and density.

Conventionally, many kinds of concretes are presently used for radiation shielding purposes since they are low-cost materials and can be molded in various shapes and sizes [9]. But concrete materials have many disadvantages; crack formation for long time exposure to nuclear radiations, decreasing in density, and the critical weakness of concretes that it can't make transparent to visible light [10]. In addition, concrete materials have a mechanical strength due to trapped water content, chemical damage, and workers cannot monitor the inside of such structures. Thus, several researchers have been focused on using glasses as novel radiation shielding materials due to their high transparency in the visible region and have the ability to absorb radiations like γ-rays and neutrons. Moreover, the physical and chemical properties of glasses can be easily altered by choosing different additive materials (such as heavy metal oxides) and changing the preparation methods. Indeed, the production of glass materials is not expensive and can easily be prepared in large sizes with high space homogeneity.

In another direction, alloys materials are formed by a combination of two or more elements (metals with metals or metals with nonmetals) with different physical and chemical properties. The

* Corresponding author. Department of Physics, Faculty of Science, Isra University, Amman, Jordan.
E-mail address: dr.mabualssayed@gmail.com (M.I. Sayyed).

main target of element combination is to enhance the mechanical properties of alloys such as tensile strength, resistance to corrosion, and hardness. These alloys material can also be utilized as an attractive radiation shielding materials [11–14].

In this study, gamma-rays shielding properties were investigated for three binary alloys of different chemical compositions of Pb–Sn, Pb–Zn, and Zn–Sn. This purpose was achieved by simulating the mass attenuation coefficient (μ/ρ) and other related shielding properties using MCNP5 code between 0.01 and 15 MeV. Moreover, the accuracy of our simulation method checked through calculating the shielding properties theoretically using the WinX-COM program. Furthermore, the efficiency of the studied binary alloys for gamma-ray shielding clarified through comparing the simulated shielding parameters with those of some commercially available shielding materials.

2. Materials and methods

2.1. Theoretical aspects

Three groups of binary alloys (Pb–Sn, Pb–Zn, and Zn–Sn) were selected from Ref. [15] to investigate their γ-radiation shielding properties. The chemical compositions and densities of the selected alloys are listed in Table 1. Alloy samples were coded as; (PS1-PS4) for the 1st group, (PZ1-PZ3) for the 2nd group, and (ZS1-ZS2) for the 3rd group.

In radiation protection, the most critical parameter is the mass attenuation coefficient, MAC (μ/ρ). The MAC is used to describe the γ-ray penetration and interaction with the materials and can be calculated theoretically through the mixture rule given as [16,17]:

$$\frac{\mu}{\rho} = \sum_i W_i \left(\frac{\mu}{\rho}\right)_i \tag{1}$$

where $(\mu/\rho)_i$ is the mass attenuation coefficient of the ith constituent element, and w_i is the weight fraction of the ith constituent component of the alloy sample.

The half-value layer (HVL) and the Mean free path (MFP) are two parameters that can signify the shielding competence of the alloy samples against γ-ray (the lower HVL and MFP, the higher shielding competence and vice versa). The HVL and MFP for the studied alloys can be calculated through equations (2) and (3):

$$HVL = \frac{\ln 2}{\mu} \tag{2}$$

$$MFP = \frac{1}{\mu} \tag{3}$$

where (μ) is the linear attenuation coefficient of the studied alloys.

The effective atomic number is another attractive shielding parameter required to describe the multi-element alloys in terms of its equivalent element and described by equation (4).

$$Z_{eff} = \frac{\sum_i f_i A_i \left(\frac{\mu}{\rho}\right)_i}{\sum_j \frac{A_j}{Z_j} \left(\frac{\mu}{\rho}\right)_j} \tag{4}$$

where f_i A_i and Z_j refer to the fractional abundance, atomic weight, and the atomic number of the ith constituent element, respectively.
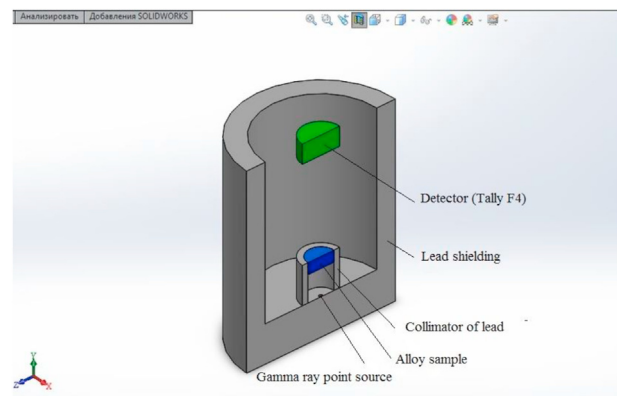
2.2. MCNP simulation

The present work deals to simulate the μ/ρ of the selected alloy samples using Monte Carlo N particle transport code MCNP- 5 code [18]. MCNP is a general code that can model γ/X-rays, neutrons, and electrons with different materials. The use of the MCNP 5 Code requires an input file that contains all information about geometry specification, elemental composition, and density of the investigated material, source specification, and tally. The geometry, as described in Fig. 1, consists of a cylinder with a thickness of 5 cm of lead was used to shield the geometry from outer space. Outside geometry was considered as void with zero importance to kill the photons in this area. The environmental filled this geometry was air, and F4 tally was used to estimate the track length of particle flux in each alloy sample. A monoenergetic disk source with a diameter of 2 cm was placed at 10 cm away from the studied alloys. The source was surrounded by a cylindrical lead collimator with a slit diameter of 2 cm. All alloy samples were defined in the input file using their densities and chemical compositions (see Table 1). The simulation was carried with 10000 histories, and the mass attenuation coefficient for different alloy samples was reported with an error of less than 1% [19–21].

Additionally, the μ/ρ for the investigated alloys was calculated using the WinXCOM program [22] to check the accuracy of the simulated results.

3. Results and discussion

The MAC values of three different series of binary alloys (Pb–Sn, Pb–Zn, and Zn–Sn) simulated in the energy range between 0.01 and 15 MeV using MCNP-5 code and those calculated by WinXcom

Table 1
Chemical compositions (fractional weight) and densities (ρ) of the (Pb–Sn, Pb–Zn, and Zn–Sn) alloys.

Sample code	Chemical composition (%)			Density ρ (g.cm^{-3})
	Lead (Pb)	Tin (Sn)	Zinc (Zn)	
Group 1				
PS1	80	20	0	9.25
PS2	60	40	0	8.07
PS3	40	60	0	8.41
PS4	20	80	0	7.08
Group 2				
PZ1	80	0	20	9.62
PZ2	50	0	50	7.36
PZ3	40	0	60	5.33
Group 3		0		
ZS1	0	20	80	6.67
ZS2	0	40	60	6.57
ZS3	0	30	70	6.87

Fig. 1. Geometry simulation used in the present study.

are listed in Table 2 and exhibited graphically in Fig. 2a, b, and c. The MAC of all studied alloys showed energy and chemical composition dependence. The MAC for all alloys in the three series tends to maximum values at low gamma-ray energy (i.e., E = 0.01 MeV) while it tends to minimum values at high gamma-ray energy (i.e., 15 MeV). Furthermore, the MCNP simulated results showed agreement with the calculated data obtained by the WinXCOM program, which ensures the accuracy of the simulated results.

Fig. 2.a depicts that the MAC of Pb−Sn alloys varied between 0.04579 and 136.7 cm^2/g. It is evident from Fig. 2.a that PS4 (0.2 Pb-0.8 Sn alloy sample) has the highest MAC (for E = 0.01 MeV). For low gamma-ray energy (0.01 < E < 0.3 MeV), the MAC for all alloys decreases rapidly with energy increase due to the domination of the photoelectric interaction in low energy region [23,24]. Moreover, two peaks were observed around 0.0292 and 0.088 MeV. The first peak is due to the K absorption edge of Sn, and its height

increases with an increase in the Sn ratio in the selected alloys. The second peak is due to the K absorption edge of Pb, and it is observed that its height decreases with a decrease in the ratio of Pb in the selected Pb−Sn alloys (first series). In the energy range between (0.5 < E < 3 MeV), the MAC values of all alloys decrease gradually due to the Compton scattering. The cross-section of this phenomenon is directly proportional to Z [25]. The MAC for all selected alloys has a very slight variation with the incident gamma-ray energy for (E > 3 MeV) due to the pair production cross-section, which proportional to log E [26]. From Table 2, we can see that in general, PS1, which contains the maximum amount of Pb, has the highest MAC. It can be concluded that increasing the Pb ratio enhances the shielding parameters for gamma-ray with medium and high energy. In contrast, the increase of the Sn ratio enhances the shielding parameters for gamma-ray with low energy only (around the K absorption edge of Sn only).

Table 2
The MAC of the studied alloys using MCNP and WinXcom.

Energy (MeV)	Mass attenuation coefficient (cm^2/g)							
	PS1		PS2		PS3		PS4	
	MCNP	WinXcom	MCNP	WinXcom	MCNP	WinXcom	MCNP	WinXcom
0,01	131,574	132,200	133,283	133,700	134,992	135,300	136,704	136,900
0,012	82,255	82,920	82,942	83,380	83,625	83,830	84,309	84,290
0,01304	95,595	143,100	133,283	124,300	81,767	105,500	74,851	86,640
0,015	98,325	98,590	85,388	85,600	72,451	72,610	59,511	59,630
0,0152	94,848	127,800	82,369	107,100	69,891	86,410	57,416	65,700
0,0153	125,938	125,800	105,496	105,400	85,048	85,020	64,598	64,610
0,01586	131,139	115,500	108,375	96,670	85,606	77,810	62,842	58,960
0,02	73,071	73,390	60,145	60,410	47,219	47,430	34,292	34,440
0,0292	35,970	27,550	35,775	22,600	31,048	17,650	24,104	12,710
0,03	33,985	32,500	34,273	34,680	30,363	36,860	23,963	39,030
0,05	8855	8573	10,106	9104	11,568	9636	11,735	10,170
0,08	2534	2541	2733	2663	3062	2785	3313	2907
0,088	1959	1998	2111	2086	2330	2173	2465	2261
0,1	4914	4775	3666	4000	3405	3226	2937	2451
0,3	0,375	0355	0,322	0308	0,260	0260	0,215	0212
0,5	0,150	0148	0,137	0134	0,123	0121	0,108	0107
0,8	0,084	0084	0,079	0080	0,075	0075	0,071	0071
1	0,066	0068	0,063	0066	0,061	0063	0,059	0061
1,5	0,050	0051	0,049	0050	0,048	0049	0,047	0048
5	0,041	0041	0,040	0040	0,038	0038	0,037	0037
10	0,047	0048	0,045	0045	0,043	0043	0,041	0041
15	0,054	0054	0,051	0051	0,048	0049	0,046	0046

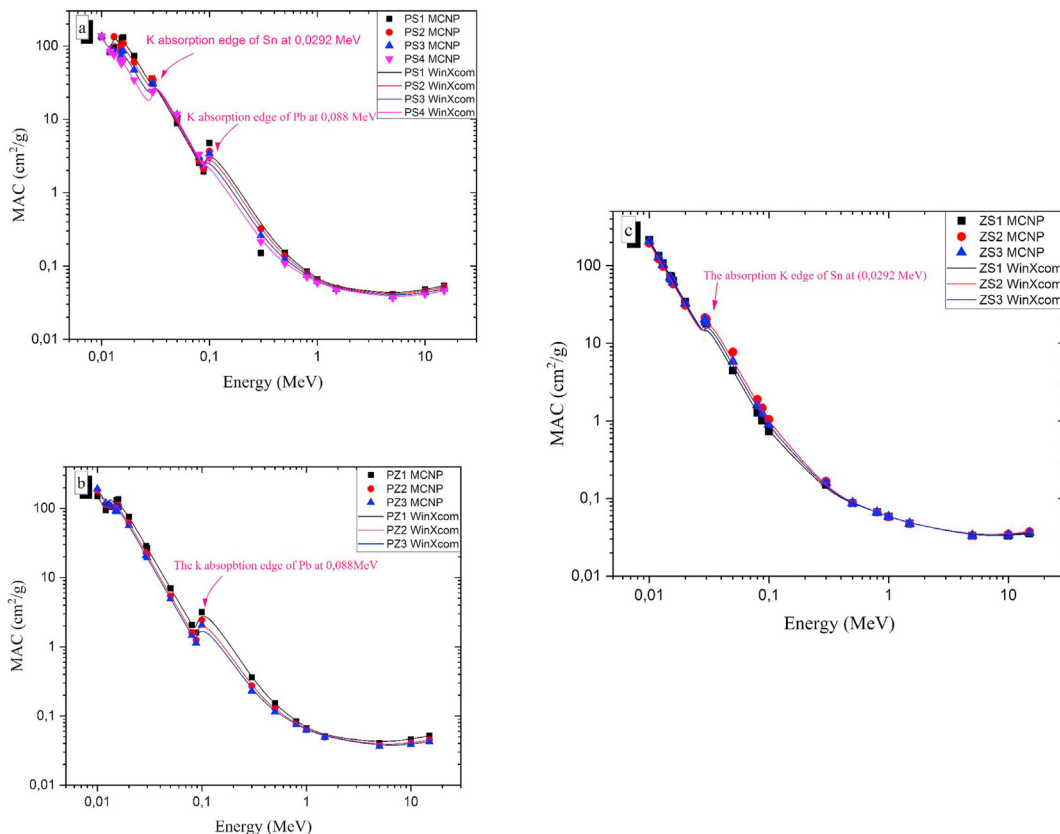| Energy (MeV)	Mass attenuation coefficient (cm^2/g)										
	PZ1		PZ2		PZ3		SZ1		SZ2		SZ3	
	MCNP	WinXcom	MCNP	WinXcom	MCNP	WinXcom	MCNP	WinXcom	MCNP	WinXcom	MCNP	WinXcom
0.01	150.604	151.100	195.498	195.200	192.079	192.100	214.525	214.100	195.498	195.200	205.013	204.700
0.012	94.543	95.360	121.844	122.100	120.476	121.100	134.125	134.500	121.844	122.100	127.990	128.300
0.01304	105.518	153.200	97.706	97.970	111.538	135.600	107.635	108.000	97.706	97.970	102.669	103.000
0.015	105.241	105.500	67.315	67.360	93.194	93.330	74.231	74.270	67.315	67.360	70.774	70.810
0.0152	101.524	134.500	64.979	64.990	89.937	106.400	71.662	71.660	64.979	64.990	68.320	68.330
0.0153	132.507	132.400	63.853	63.850	104.750	104.700	70.420	70.410	63.853	63.850	67.138	67.130
0.01586	137.094	121.500	57.937	57.950	103.467	95.660	63.893	63.900	57.937	57.950	60.916	60.920
0.02	76.238	76.540	30.863	30.900	56.715	56.870	34.028	34.050	30.863	30.900	32.446	32.470
0.0292	28.595	28.600	21.348	10.910	20.811	20.810	19.101	11.960	21.348	10.910	20.397	11.440
0.03	26.646	26.670	20.576	23.730	19.364	19.370	17.845	17.900	20.576	23.730	18.432	20.810
0.05	6.978	7.012	7.700	6.015	4.937	4.952	4.457	4.454	7.700	6.015	5.794	5.234
0.08	2.063	2.103	1.887	1.713	1.450	1.470	1.275	1.275	1.887	1.713	1.586	1.494
0.088	1.602	1.661	1.459	1.339	1.134	1.163	1.002	1.002	1.459	1.339	1.234	1.170
0.1	3.170	4.539	1.042	0.969	2.047	2.518	0.734	0.733	1.042	0.969	0.889	0.851
0.3	0.364	0.345	0.167	0.134	0.229	0.230	0.151	0.124	0.167	0.134	0.160	0.129
0.5	0.152	0.146	0.088	0.088	0.115	0.115	0.086	0.086	0.088	0.088	0.087	0.087
0.8	0.084	0.084	0.066	0.067	0.075	0.075	0.066	0.067	0.066	0.067	0.066	0.067
1	0.066	0.069	0.058	0.059	0.062	0.064	0.058	0.059	0.058	0.059	0.058	0.059
1.5	0.050	0.051	0.047	0.048	0.049	0.050	0.048	0.048	0.047	0.048	0.047	0.048
5	0.040	0.041	0.033	0.034	0.036	0.036	0.033	0.033	0.033	0.034	0.033	0.033
10	0.046	0.046	0.035	0.035	0.039	0.039	0.033	0.033	0.035	0.035	0.034	0.034
15	0.052	0.052	0.037	0.037	0.043	0.043	0.035	0.035	0.037	0.037	0.036	0.036

Fig. 2. The energy dependence of MAC for (a) Pb–Sn alloys, (b) Pb–Zn alloys and (c) Zn–Sn alloys.

Fig. 2b shows the variation of the MAC for Pb–Zn alloys with the incident energy. The MAC for Pb–Zn alloys varied between 0.04258 and 192.0793 cm^2/g. The mode in which the gamma photons interact with the Pb–Zn alloys can be discussed, like in the previous curve (i.e., for Pb–Sn alloys). It is observed that there is one peak at 0.088 MeV due to the K absorption edges of Pb and its intensity increases with increase Pb ratio for Pb–Zn alloys. No beaks observed for the Zn element because it occurs at 0.0096 MeV, while we selected energy range started from 0.01 MeV. Also, one can see that the MAC increases with an increase in the Zn ratio at low energy while in high energy, the MAC increases with an increase in the Pb ratio.

The MAC of the Zn–Sn alloys is illustrated in Fig. 2c in which the MAC varied between 0.03525 and 214.5249 cm^2/g. The highest and lowest MAC obtained for ZS1 alloy. As we found in Fig. 2b, only one peak appears at 0.0292 MeV due to the K absorption edge of Sn, while no peaks are found from the Zn element.

The simulated MAC was then used to calculate two essential shielding parameters (HVL and MFP), which describe the penetration of the incident gamma-ray. The variation of the HVL with the incident gamma-ray energy is illustrated in Fig. 3, which reveals that the thinner HVL is found for PZ1 and varied between 0.000478 and 1.3913 cm, while the thicker HVL is obtained for PZ3 and varied between 0.00068 and 3.0542 cm. Firstly, at low gamma-ray energies between (0.01< E < 0.3 MeV), the HVL for all studied alloys is increased rapidly with the incident gamma-ray energy. Then, at intermediate gamma-ray energies between (0.04 < E < 3 MeV), the HVL increases gradually due to the Compton scattering. Finally, at higher gamma-ray energy values (E > 3 MeV), the HVL has a small variation with the incident gamma-ray energy due to the pair production, where the cross-section of this mechanism is proportional to log E [27,28].
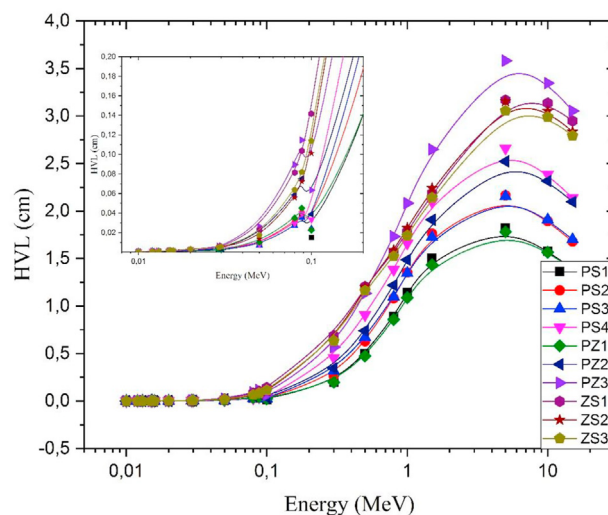

Fig. 3. Variation of the HVL with the incident gamma ray energy for the prepared alloys.

The MFP of the proposed alloys is illustrated in Fig. 4, which reveals that the lowest MFP is obtained for PZ1 alloy and varied between 0.00069 and 2.0041 cm. It is also clear that the highest MFP is achieved for alloy PZ3 and varied between 0.0009 and 4.4063 cm. The mechanism in which MFP changed with the incident energy is similar to the early discussed in the HVL curve.

According to the HVL and MFP curves, we can conclude that a thinner thickness of alloy PZ1 is required for shielding against
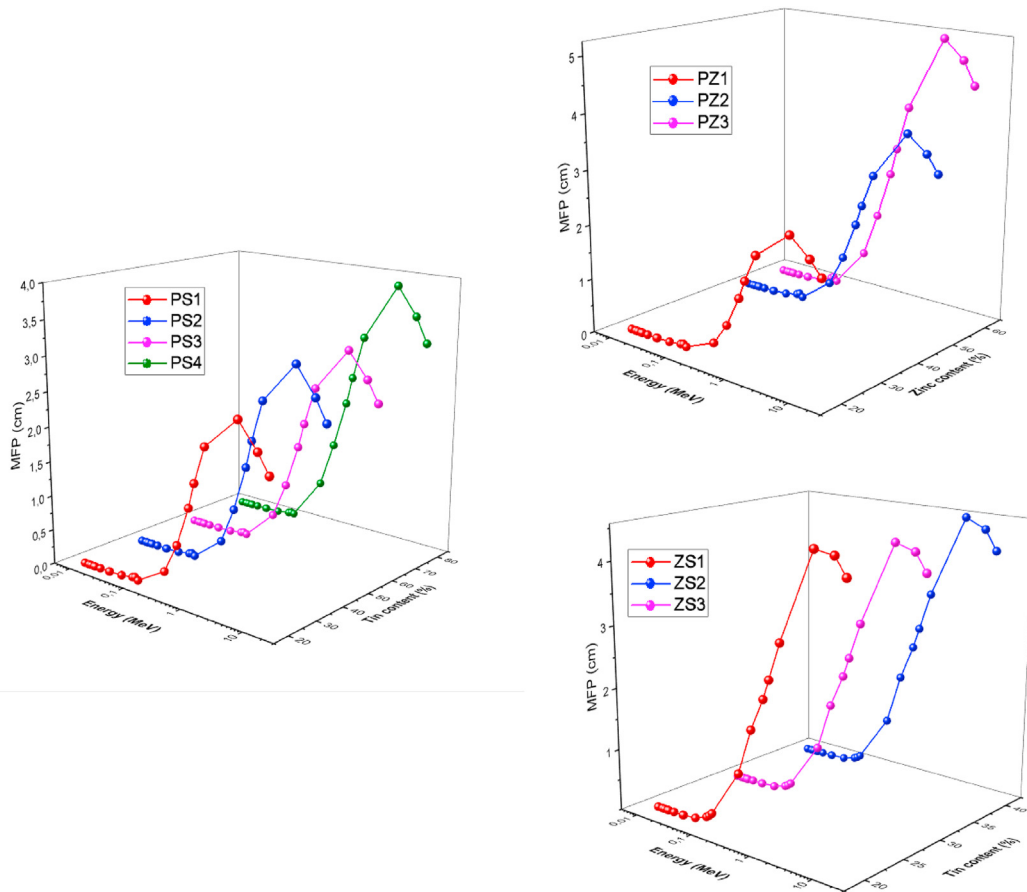
Fig. 4. Variation of the MFP of various prepared alloys with the incident energy.

gamma radiation for the investigated energies, while a thicker layer of alloy PZ3 necessary for protecting against gamma radiation with the same investigated energies.

The effective atomic number (Z_{eff}) is a shielding factor calculated through the atomic and electron cross-section of the investigated alloys. Fig. 5a, b, and c show the dependence of Z_{eff} for all studied alloys on the incident gamma-ray energy. Fig. 5a reveals that the Z_{eff} for all Pb–Sn alloys varied between 74.2 and 80.3, 67.2–77.8, 60.9–73.9, and 55.2–66.8 for PS1, PS2, PS3, and PS4, respectively. Also, from Fig. 5, the maximum Z_{eff} values of Pb–Sn alloys are found at low gamma-ray energy between (0.01304 and 0.01586 MeV). In contrast, the minimum values were obtained for energy range between (0.03 and 0.088 MeV), and there is no noticeable variation in Z_{eff} with high energy (for E > 3 MeV). It is worth mention that at low energy (i.e., 0.01< E < 0.01586 MeV), the Z_{eff} for alloys increases with increasing energy, and this can be explained based on the K-edge absorption of Sn and L-edge absorption of Pb. Z_{eff} decreases with the growth of the incident energy due to the photoelectric effect, where the cross-section is inversely proportional to the energy (with $E^{-3.5}$). After that, there is a sudden jump at energy E = 0.088 MeV, which can be explained as the K-edge absorption of Pb [29]. It also clear that the Z_{eff} decreases with a decrease in the Pb ratio in the Pb–Sn alloys (first series).

The Z_{eff} variation with incident gamma energy for Pb–Zn alloys is illustrated in Fig. 5b. The Z_{eff} for these alloys are found in the rage of 67.5–81.0, 50.4–78.2, and 45.7–76.5 for PZ1, PZ2, and PZ3, respectively. The minimum and maximum Z_{eff} for alloys is reported at 0.01 MeV and for gamma-ray energy between 0.1 and 0.3 MeV, respectively. For low gamma-ray energy (i.e., 0.01 < E < 0.01568),

the Z_{eff} for alloys is increased with energy, which can be explained as the L1, L2, and L3 absorption edges of lead. Then, in the energy range between 0.02 and 0.08 MeV, the Z_{eff} for all alloys is nearly independent of the incident energy. After that, Z_{eff} suddenly increased at E = 0.088 MeV due to the K edge of Pb like that observed for Pb–Sn alloys. Also, no significant variation in Z_{eff} is noticed for E > 3 MeV due to the pair production cross-section. Fig. 5b also shows that the Z_{eff} of Pb–Zn alloys increases with increasing the Pb ratio.

Fig. 5c shows that the Z_{eff} of Zn–Sn alloys varied in the range between 32.7 and 40.0, 35.9–44.5, and 34.2–42.6 for ZS1, ZS2, and ZS3, respectively. The minimum values of Z_{eff} were also obtained at low energy (i.e., at 0.01 MeV) like Pb–Zn alloys but the maximum values obtained for energy between 0.03 and 0.1 MeV. It is also clear that the Z_{eff} increases with an increase in the ratio of Sn in Zn–Sn alloys. One can conclude that the Pb and Sn additive enhance the Z_{eff} for Pb–Zn, Pb–Sn, and Zn–Sn alloys. Also, it is clear that the alloy samples in the first group have higher Z_{eff} values than the alloys in the third group due to the high content of Pb in these samples.

In order to examine the selected alloys for practical utilization, it is imperative to compare the shielding properties of the studied alloys to some standard shielding materials. Figs. 6–8 shows the comparison of the MAC, HVL, and MFP for the investigated alloys PS1, PZ1, and ZS2 with other commercially available radiation shielding materials such as (ordinary concrete [30], borate glass 100 $Na_2B_4O_7$ [31], and RS-360 (F2) glass [32].

Fig. 6 displays that the MAC of the alloy samples PS1 and PZ1 is higher than the MAC of ordinary concretes, borate glass, and RS-
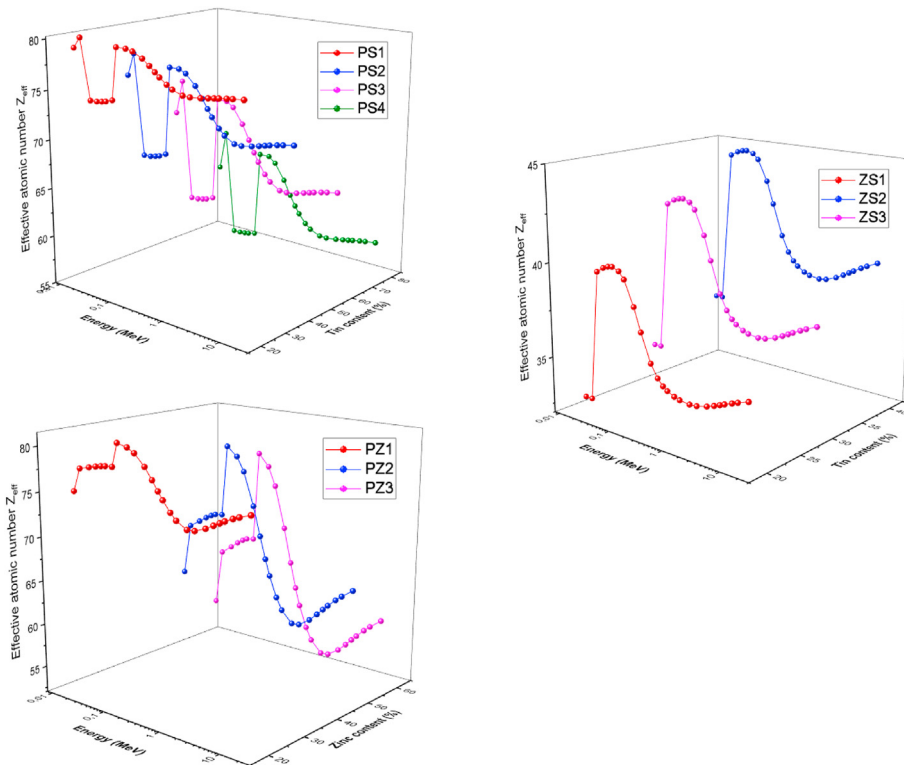
Fig. 5. The variation of Z_{eff} for (a) Pb−Sn alloys, (b) Pb−Zn alloys and (c) Zn−Sn alloys with the incident gamma ray energy.

Fig. 6. The MAC for PS1, PZ1 and SZ2 alloys in comparison with some different shielding materials.
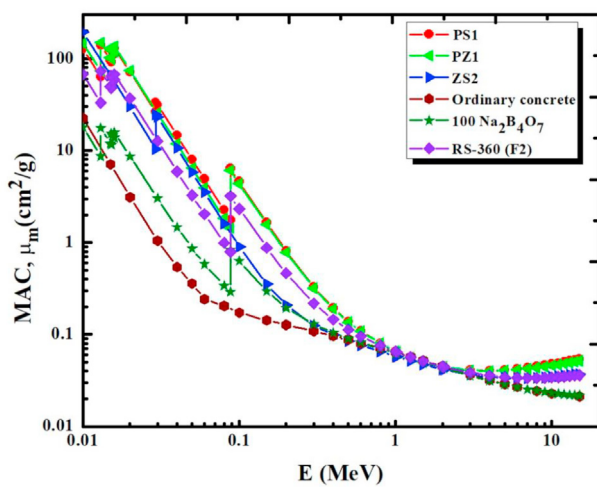

Fig. 7. The HVL for PS1, PZ1 and SZ2 alloys in comparison with some different shielding materials.

360 (F2) glass at an energy between 0.01 and 15 MeV. It is also clear that the ZS2 alloy has MAC equal to that obtained for RS-360 (F2) and higher than the MAC of the ordinary concrete and borate glass.

According to Figs. 7 and 8, the three alloys PS1, PZ1, and ZS2 have a lower HVL and MFP than some commercial radiation shielding materials.

Exposure buildup factor for the selected alloys computed between 0.015 and 15 MeV, as illustrated in Fig. 9-a for PS1, while the EBF for the remaining alloys are included in supplementary data in Figure S (b-j) using the geometry progression (G-P) fitting Method. Fig. 9-a and Fig.S (b-d) refers to the exposure buildup factor variation with the incident gamma-ray energy for the Pb−Sn alloys at
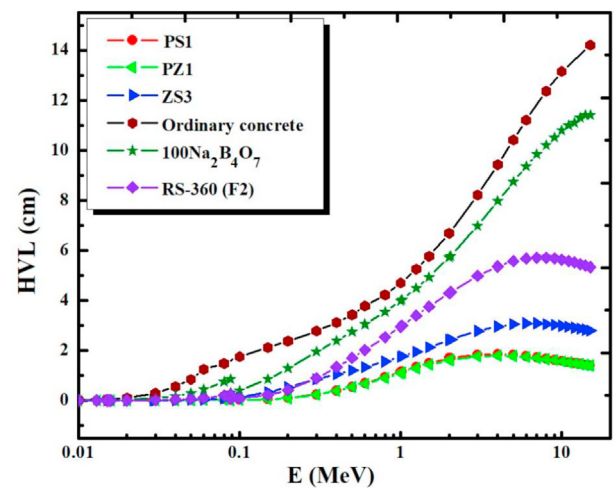
penetration depth between 0.5 and 40 mfp. The EBF tends to minimum values at low gamma-ray energy due to the photoelectric interaction, which removes the energy of the incident photons and prevents its accumulation inside the shielding materials and the EBF for all alloys is nearly constants at various penetration depth. We can observe in Fig. 9 (a and b), two high peaks appear at 0.03 and 0.088 MeV due to the L1 and K absorption edges of the lead, which represent about 80 and 60% of the two alloys PS1 and PS2, respectively. For alloys PS3 and PS4 showed in Fig S (c and d), it is clear that the peak of lead at 0.088 MeV disappeared, and we have one peak with resulting from the overlapping of L1 absorption beak of lead and K absorption peak of tin at 0.0292 MeV and the amplitude of this
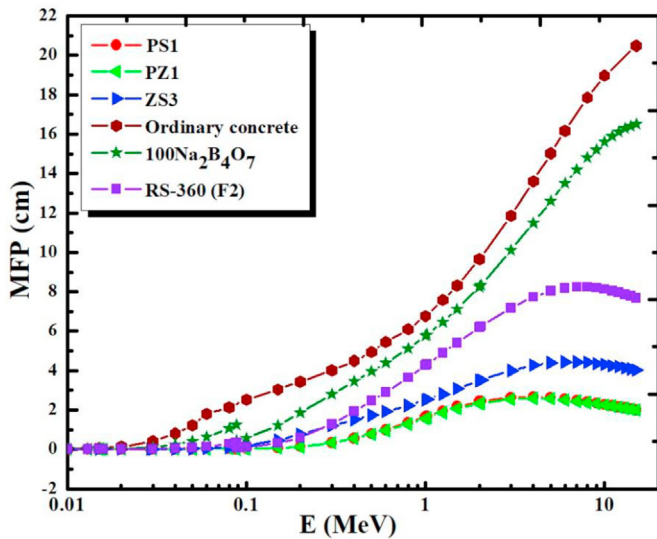
Fig. 8. The MFP for PS1, PZ1 and SZ2 alloys in comparison with some different shielding materials.
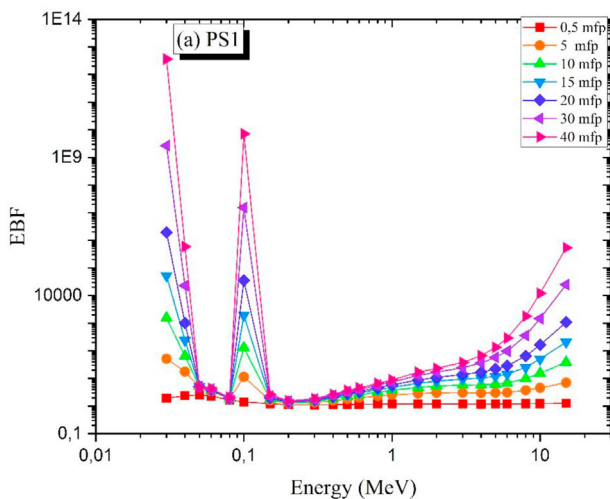

Fig. 9. The exposure buildup factor for PS1.

peak increases with increase the Sn content in the alloy samples. For intermediate gamma-ray energy (0.03 < E < 5 MeV), the EBF for all samples increases gradually with increase the incident gamma-ray photons due to the Compton scattering interaction, which helps the photon to accumulate inside the alloy samples. For high gamma-ray energies (E > 5 MeV), we find that the EBF has an increasing trend exceptionally high penetration depth for (30 and 40 mfp) due to the pair production interaction, which duplicates the number of photons inside the alloy material, especially for high energies and penetration depth.

The variation of EBF of Pb–Zn alloys with the incident gamma photon and penetration depth showed in Fig. S (e-g). The variation of the EBF of Pb–Zn with the incident gamma-ray energy is similar to the EBF to Pb–Sn alloys, but there are only two differences. The first difference, the peaks appear in Fig. S (e-g), are for the L1 and K absorption photons of lead, and there are no absorption peaks that appeared for Zn because of the k absorption peaks of Zn occurs at 0.009659 MeV. The parameters used for EBF calculation was found in the energy range between 0.015 and 15 MeV the second

difference, the EBF for Pb–Zn alloys is lower than that for Pb–Sn alloys for all studied energies and penetration depth.

The EBF of Sn–Zn alloys with gamma photon energies at different penetration depth illustrated Fig.S (h-j). There is no sharp peak at low energy due to the K-absorption edges of tin at 0.0292 MeV. We can conclude that the addition of tin and zinc for lead reduces the EBF of the Pb–Sn and Pb–Zn binary alloys. The lowest EBF in the present study was achieved for the Sn–Zn alloys.

Finally, one can conclude that the PS1, PZ1, and ZS2 have the best shielding parameters in this study, and also their shielding parameters are better than the commercially standard and available radiation shielding materials, namely ordinary concrete, borate glass (100 Na_2B_4O), and RS-360 (F2) glass. The selected alloys can be used as effective radiation shielding materials against gamma-ray with energies between 0.01 and 15 MeV.

4. Conclusion

In the present study, γ-ray shielding properties for some binary alloy samples of different compositions of Pb–Sn, Pb–Zn, and Zn–Sn were investigated. The aim was achieved by simulating the mass attenuation coefficients, MAC ($μ/ρ$) using MCNP-5 code, and WinXCOM program in photon energy range 0.01–15 MeV. The related shielding parameters (HVL), (MFP), and (Z_{eff}) have been evaluated and compared with some commercially available radiation shielding materials. The obtained results reveal that:

1. The MAC for the Pb–Sn, Pb–Zn, and Zn–Sn alloys were found in the range of 0.04579–136.7, 0.04258–192.0793, and 0.03525–214.5249 cm^2/g.
2. For the first alloys series, the thinner HVL is found for PZ1 and varied between 0.000478 and 1.3913 cm, while the thicker HVL is obtained for PZ3 and varied between 0.00068 and 3.0542 cm.
3. The Z_{eff} for all Pb–Sn alloys varied in the range 74.2–80.3, 67.2–77.8, 60.9–73.9, and 55.2–66.8 for PS1, PS2, PS3, and PS4, respectively, while for the Pb–Zn alloys in the rage of 67.5–81.0, 50.4–78.2, and 45.7–76.5 for PZ1, PZ2, and PZ3, respectively. Also, the Zeff for the Zn–Sn alloys varied in the range between 32.7 and 40.0, 35.9–44.5, and 34.2–42.6 for ZS1, ZS2, and ZS3, respectively.
4. The comparison between the radiation shielding properties for the selected alloys showed that the MACs of the investigated alloys PS1 and PZ1 are higher than the MAC of ordinary concretes, borate glass, and RS-360 (F2) glass at gamma-photon energy between 0.01 and 15 MeV. The ZS2 alloy has MAC equal to that obtained for RS-360 (F2) and higher than the MAC of the ordinary concrete and borate glass.
5. The EBF decreases with increase Sn and Zn concentrations for all selected alloys
6. The Pb and Sn additive enhance the Z_{eff} for Pb–Zn, Pb–Sn, and Zn–Sn alloys.

Generally, results revealed that the PS1, PZ1, and ZS2 alloys have the best shielding parameters in this study. Their shielding parameters are better than the commercially standard and available radiation shieldings materials such as ordinary concrete, borate glass (100 Na_2B_4O), and RS-360 (F2) glass. Thus, the investigated alloys can be used as effective radiation shielding materials against gamma-ray with energies between 0.01 and 15 MeV.

Declaration of competing interest

The authors declare that they have no known competing financial interests or personal relationships that could have appeared to influence the work reported in this paper.

Appendix A. Supplementary data

Supplementary data to this article can be found online at https://doi.org/10.1016/j.net.2021.02.021.

References

[1] E.S.A. Waly, M.A. Fusco, M.A. Bourham, Gamma-ray mass attenuation coefficient and half value layer factor of some oxide glass shielding materials, Ann. Nucl. Energy 96 (2016) 26–30, https://doi.org/10.1016/j.anucene.2016.05.028.

[2] K.A. Mahmoud, O.L. Tashlykov, A.F. El Wakil, I.E. El Aassy, Aggregates grain size and press rate dependence of the shielding parameters for some concretes, Prog. Nucl. Energy 118 (2020) 103092, https://doi.org/10.1016/j.pnucene.2019.103092.

[3] M.I. Sayyed, R. El-Mallawany, Shielding properties of (100-x) TeO$_2$-(x)MoO$_3$ glasses, Mater. Chem. Phys. 201 (2017) 50–56.

[4] R. El-Mallawany, M.I. Sayyed, Comparative shielding properties of some tellurite glasses: part 1, Physica B Condens. Matter 539 (2018) 133–140.

[5] A.S. Abouhaswa, Y.S. Rammah, M.I. Sayyed, H.O. Tekin, Synthesis , structure , optical and gamma radiation shielding properties of, Composites Part B 172 (2019) 218–225, https://doi.org/10.1016/j.compositesb.2019.05.040.

[6] Y. Al-Hadeethi, M.I. Sayyed, BaO–Li$_2$O–B$_2$O$_3$ glass systems: potential utilization in gamma radiation protection, Prog. Nucl. Energy 129 (2020) 103511.

[7] Y. Al-Hadeethi, M.I. Sayyed, M. Hiba, L. Rimondin, X-ray photons attenuation characteristics for two tellurite-based glass systems at dental diagnostic energies, Ceram. Int. 46 (2020) 251–257.

[8] T. Singh, A. Kaur, J. Sharma, P.S. Singh, Engineering Science and Technology , an International Journal Gamma rays ' shielding parameters for some Pb-Cu binary alloys, Eng. Sci. Technol. Int. J. 21 (2018) 1078–1085, https://doi.org/10.1016/j.jestch.2018.06.012.

[9] A.M. Abu El-soad, M.I. Sayyed, K.A. Mahmoud, Ş. Erdem, E.G. Kovaleva, Simulation studies for gamma ray shielding properties of Halloysite nanotubes using MCNP-5 code, Appl. Radiat. Isot. 154 (2019) 1–6, https://doi.org/10.1016/j.apradiso.2019.108882.

[10] S. Kaur, K.J. Singh, Annals of Nuclear Energy Investigation of lead borate glasses doped with aluminium oxide as gamma ray shielding materials, Annu. Nucl. Energy 63 (2014) 350–354, https://doi.org/10.1016/j.anucene.2013.08.012.

[11] F. Akman, M.R. Kaçal, M.I. Sayyed, H.A. Karataş, Study of gamma radiation attenuation properties of some selected ternary alloys, J. Alloys Compd. 782 (2019) 315–322, https://doi.org/10.1016/j.jallcom.2018.12.221.

[12] S. Kaur, A. Kaur, P.S. Singh, T. Singh, Progress in Nuclear Energy Scope of Pb-Sn binary alloys as gamma rays shielding material, Prog. Nucl. Energy 93 (2016) 277–286, https://doi.org/10.1016/j.pnucene.2016.08.022.

[13] J. Singh, H. Singh, J. Sharma, T. Singh, P.S. Singh, Fusible alloys : a potential candidate for gamma rays shield design, Prog. Nucl. Energy 106 (2018) 387–395, https://doi.org/10.1016/j.pnucene.2018.04.002.

[14] M.I. Sayyed, Faras Q. Mohammed, Eloic Lacomme, Kawa M. Kaky, Mayeen Uddin Khandaker, Mohammad Rashed Iqbal Faruque, Evaluation of radiation shielding features of Co and Ni-based superalloys using MCNP-5 code: potential use in nuclear safety, Appl. Sci. 10 (2020), https://doi.org/10.3390/app10217680.

[15] R. Sharma, J.K. Sharma, T. Kaur, T. Singh, J. Sharma, P.S. Singh, Experimental investigation of effective atomic numbers for some binary alloys, Nucl. Eng. Technol. 49 (2017) 1571–1574, https://doi.org/10.1016/j.net.2017.06.007.

[16] K.A. Mahmoud, O.L. Tashlykov, A.F. El Wakil, H.M.H. Zakaly, I.E. El Aassy, Investigation of radiation shielding properties for some building materials reinforced by Basalt powder, AIP Conf. Proc. 2174 (2019), https://doi.org/10.1063/1.5134187.

[17] K.A. Mahmoud, E. Lacomme, M.I. Sayyed, Ö.F. Özpolat, O.L. Tashlykov, Investigation of the gamma ray shielding properties for polyvinyl chloride reinforced with chalcocite and hematite minerals, Heliyon 6 (2020), e03560.

[18] RSICC, Computer Code Collection, MCNPX User's Manual Version 2.4.0. Monte Carlo N-Particle Transport Code System for Multiple and High Energy Applications, 2002.

[19] Y.S. Rammah, F.I. El-Agawany, K.A. Mahmoud, A. Novatski, R. El-Mallawany, Role of ZnO on TeO$_2$.Li$_2$O.ZnO glasses for optical and nuclear radiation shielding applications utilizing MCNP5 simulations and WINXCOM program, J. Non-Cryst. Solids 544 (2020), 120162, https://doi.org/10.1016/j.jnoncrysol.2020.120162.

[20] M.I. Sayyed, A.A. Ali, M.H.A. Mhareb, K.A. Mahmoud, K.M. Kaky, Baki, M.A. Mahdi, Novel tellurite glass (60-x)TeO2–10GeO$_2$ -20ZnO–10BaO - xBi$_2$O$_3$ for radiation shielding, J. Alloys Compd. 844 (2020) 155668, https://doi.org/10.1016/j.jallcom.2020.155668.

[21] K.M. Kaky, M.I. Sayyed, A.A. Ali, M.H.A. Mhareb, K.A. Mahmoud, S.O. Baki, Germanate oxide impacts on the optical and gamma radiation shielding properties of TeO$_2$-ZnO-Li$_2$O glass system, J. Non-Cryst. Solids 546 (2020) 120272, https://doi.org/10.1016/j.jnoncrysol.2020.120272.

[22] D.S.Z.M.J. Berger, J.H. Hubbell, S.M. Seltzer, J. Chang, J.S. Coursey, R. Sukumar, XCOM: Photon Cross Sections Database, 2010, https://doi.org/10.18434/T48G6X.

[23] Aljawhara H. Almuqrin, M.I. Sayyed, Radiation shielding characterizations and investigation of TeO2–WO3–Bi2O3 and TeO2–WO3–PbO glasses, Appl. Phys. A 127 (2021), https://doi.org/10.1007/s00339-021-04344-9.

[24] K.A. Mahmoud, M.I. Sayyed, O.L. Tashlykov, Gamma ray shielding characteristics and exposure buildup factor for some natural rocks using MCNP-5 code, Nucl. Eng. Technol. 51 (2019) 1835–1841, https://doi.org/10.1016/j.net.2019.05.013.

[25] M.I. Sayyed, M.G. Dong, H.O. Tekin, G. Lakshminarayana, M.A. Mahdi, Comparative investigations of gamma and neutron radiation shielding parameters for different borate and tellurite glass systems using WinXCom program and MCNPX code, Mater. Chem. Phys. 215 (2018) 183–202, https://doi.org/10.1016/j.matchemphys.2018.04.106.

[26] U. Kaur, J.K. Sharma, P.S. Singh, T. Singh, Comparative studies of different concretes on the basis of some photon interaction parameters, Appl. Radiat. Isot. 70 (2012) 233–240, https://doi.org/10.1016/j.apradiso.2011.07.011.

[27] M.I. Sayyed, M.H.M. Zaid, N. Effendy, K.A. Matori, H.A. Sidek, E. Lacomme, K.A. Mahmoud, M.M. AlShammari, The influence of PbO and Bi$_2$O$_3$ on the radiation shielding and elastic features for different glasses, J. Mater. Res. Technol. 9 (2020) 8429–8438, https://doi.org/10.1016/j.jmrt.2020.05.113.

[28] A.S. Abouhaswa, M.I. Sayyed, K.A. Mahmoud, Y. Al-Hadeethi, Direct influence of mercury oxide on structural, optical and shielding properties of a new borate glass system, Ceram. Int. 46 (2020) 17978–17986, https://doi.org/10.1016/j.ceramint.2020.04.112.

[29] M.I. Sayyed, Bismuth modified shielding properties of zinc boro-tellurite glasses, J. Alloys Compd. 688 (2016) 111–117, https://doi.org/10.1016/j.jallcom.2016.07.153.

[30] I.I. Bashter, A.S. Makarious, E.S. Abdo, Investigation of hematite-serpentine and ilmenite-limonite concretes for reactor radiation shielding, Ann. Nucl. Energy 23 (1996) 65–71, https://doi.org/10.1016/0306-4549(95)00011-G.

[31] V.P. Singh, N.M. Badiger, Shielding efficiency of lead borate and nickel borate glasses for gamma rays and neutrons 1, Glass Phys. Chem. 41 (2015) 276–283, https://doi.org/10.1134/S1087659615030177.

[32] (〈 http://www.schott.com/advanced_optics/english/products/optical-materials/special-materials/radiation-shielding-glasses/index.html 〉 , n.d.).